processes

MDPI

Article

Research and Application of Gas Drainage Negative Pressure Regulation Method Considering Permeability Differences

Xiaoyu Cheng [1,*], Cheng Cheng [1], Hui Wang [2], Lu Xiao [1,3] and Xingying Ma [1]

[1] China Coal Energy Research Institute Co., Ltd., Xi'an 710054, China
[2] Shaanxi Qinan Coal Mine Safety Evaluation Services Limited, Xi'an 710054, China
[3] Research Center of Fluid Machinery Engineering and Technology, Jiangsu University, Zhenjiang 212013, China
* Correspondence: chengxiaoyu@chinacoal.com

Abstract: This study investigates a dynamic regulation strategy for intelligent gas drainage negative pressure using a comprehensive approach involving numerical simulations, intelligent algorithms, and field experiments. In the numerical simulation component, a permeability evolution model was developed to characterize the area in front of the mining face. Simulations were performed under three negative pressure settings (13 kPa, 18 kPa, and 25 kPa) to investigate the relationships among drainage negative pressure, gas concentration, and flow rate. For the intelligent algorithm, a Long Short-Term Memory (LSTM) prediction model was developed to forecast drainage negative pressure. Based on the predictions, a dynamic regulation strategy for intelligent gas drainage negative pressure was formulated. For field validation, a 120-day in situ experiment was carried out. Intelligent control valves and monitoring instruments were deployed across various sections of the coal seam ahead of the mining face, validating the proposed regulation strategy. The results indicate that permeability is highest in the pressure-relief zone ahead of the mining face and lowest in the stress concentration zone. In the original stress zone, which is unaffected by mining disturbances, the permeability remains unchanged. Drainage negative pressure is positively correlated with gas flow rate, but negatively correlated with gas concentration. In the stress concentration zone, when drainage negative pressure reaches 25 kPa, permeability ceases to be the dominant factor influencing gas flow. At this stage, the pressure gradient between the gas in coal fractures and the drainage system becomes the primary driving force for gas flow. The intelligent dynamic regulation strategy for gas drainage, underpinned by the LSTM prediction model, demonstrated strong performance in field applications. Following intelligent regulation, gas concentrations in various regions showed significant improvement. The findings of this study actively contribute to the advancement of intelligent gas drainage technology.

Keywords: permeability; drainage negative pressure; drainage concentration; negative pressure dynamic regulation

check for updates

Academic Editor: Albert Ratner

Received: 21 March 2025
Revised: 15 April 2025
Accepted: 16 April 2025
Published: 19 April 2025

Citation: Cheng, X.; Cheng, C.; Wang, H.; Xiao, L.; Ma, X. Research and Application of Gas Drainage Negative Pressure Regulation Method Considering Permeability Differences. *Processes* **2025**, *13*, 1236. https://doi.org/10.3390/pr13041236

Copyright: © 2025 by the authors. Licensee MDPI, Basel, Switzerland. This article is an open access article distributed under the terms and conditions of the Creative Commons Attribution (CC BY) license (https://creativecommons.org/licenses/by/4.0/).

1. Introduction

A considerable number of mines in China are characterized by low permeability, high gas content, and proneness to outbursts, posing serious risks such as gas over-limit incidents, outbursts, and explosions during mining operations [1–3]. Moreover, large-scale gas emissions contribute significantly to environmental pollution [4,5]. Gas drainage serves as a crucial measure for both gas disaster prevention and environmental management. Negative pressure drainage leverages the pressure gradient induced by suction to facilitate

gas desorption from the coal seam and its subsequent flow into the drainage pipeline, effectively reducing gas content and pressure within the seam [6–11]. Coal seam permeability is also a key factor influencing gas migration. With the advancement of intelligent mining, smart gas drainage has emerged as an integral component [12–16]. Precise regulation of negative pressure plays a pivotal role in enabling intelligent gas drainage. Therefore, investigating the evolution of coal seam permeability and developing a dynamic negative pressure regulation strategy is of great theoretical and practical significance [17,18].

Cheng Yuanping et al. [19] developed a gas–solid coupled model of gas migration, incorporating matrix pseudo-steady-state diffusion, fracture seepage, permeability evolution, and coal deformation, to analyze the influence of diffusion and seepage on gas transport. Luo Zhiqiang et al. [20] proposed a multifactorial model incorporating intelligent algorithms to accurately forecast gas concentration. Wang Zhaofeng et al. [21] suggested that increasing negative pressure enhances drainage efficiency, though its effect on gas volume becomes marginal over extended drainage durations. Zhou Fubao et al. [22] found that higher negative pressures are associated with increased gas leakage from drainage boreholes. In summary, extensive theoretical research has been conducted on negative pressure regulation. However, current technologies still suffer from limitations, including imprecise control and the lack of real-time regulation capabilities. Xia Tongqiang et al. [23] established safety and efficiency criteria for gas drainage, proposed an adaptive control strategy, and developed a corresponding model based on particle swarm optimization. Liu Jun et al. [24] developed a theoretical model based on coupled coal seam seepage and borehole gas flow to quantify gas pressure variations under different influencing factors. Li Chuantian et al. [25] examined drainage effectiveness via gas pressure analysis and determined the pressure distribution around drainage boreholes. Zhou Aitao et al. [26] developed a three-dimensional gas distribution model for the goaf, assessing the effects of borehole spacing and negative pressure on drainage performance. Gao Han et al. [27] proposed a fully coupled gas–air flow model to evaluate the impacts of drainage duration, pressure levels, and leakage on gas concentration. Zhou Aitao et al. [28] proposed a graph-theory-based gas drainage network model, grounded in an air–gas mixed flow framework.

Furthermore, the influence of mining-induced disturbances on negative pressure regulation remains insufficiently studied. In response to these challenges, this study derives a permeability evolution model for the zone ahead of the mining face. The study also simulates the interrelationship between drainage pressure, gas flow rate, and concentration. Building on these results, an LSTM-based prediction algorithm was employed to formulate a dynamic regulation strategy for intelligent gas drainage. Finally, field experiments were conducted to validate the applicability of the proposed intelligent gas drainage regulation strategy.

2. Coal Permeability Evolution and Gas Flow Equation

2.1. Permeability and Porosity Evolution Equation of Coal Body Under Mining Disturbance

The deformation of the coal body within the seam is affected by various environmental factors, leading to corresponding changes in the pore structure of the coal matrix. During actual coal face mining, porosity and permeability exhibit dynamic variability. Therefore, deriving evolution equations for porosity and permeability is essential for developing a gas–solid coupling model of the mined coal seam [29].

The porosity evolution equation of the coal body, incorporating the initial porosity, is expressed as follows:

$$\phi = 1 - \frac{1-\phi_0}{1+\varepsilon_v}\left(1 + \frac{\varepsilon_s}{1-\phi_0} - K_Y \Delta p + \gamma \Delta T\right) \quad (1)$$

In the equation:

ϕ is the porosity of the coal body, %;

ϕ_0 is the initial porosity of the coal body, %;

ε_v is the total volumetric strain of the coal body, as the change in volume per unit volume of the object;

ε_s is the gas adsorption expansion strain of the coal body;

K_Y is the material volumetric compression coefficient, MPa^{-1}; $K_Y = 3(1-2v)/E$; its value is negative because compression leads to a reduction in volume;

E is the elastic modulus of the coal, GPa;

v is the Poisson's ratio of the coal;

Δp is the change in environmental gas pressure, MPa;

γ is the thermal expansion coefficient of the coal body, measured as the degree of thermal expansion of the coal body;

ΔT is the change in environmental absolute temperature, K.

Neglecting temperature fluctuations and gas adsorption-induced expansion, and assuming that the total surface area of coal particles per unit volume remains constant under stress-induced deformation, $\gamma(p) = 0$, the dynamic permeability evolution equation is derived as follows:

$$k = \frac{k_0}{1+\varepsilon_v}\left[1 + \frac{\varepsilon_v}{\phi_0} + \frac{(1-\phi_0)K_Y \Delta p}{\phi_0}\right]^3 \tag{2}$$

In the equation:

k_0 is the initial permeability of the coal body, m^2.

2.2. Gas–Air Flow Equation

A cubic microflow system is adopted as the representative elementary volume (REV) of the coal body seepage system for the formulation of the gas flow equation, as illustrated in Figure 1. Over a short time interval, Δt, and in accordance with the law of mass conservation, the net gas mass flux into and out of the elementary unit, combined with any internal mass sources, equals the total change in gas mass within the system.

$$\frac{\partial Q}{\partial t} = \left(\frac{c\rho_c \rho_0 ab}{(1+bp)^2} + \beta\phi\right)\frac{\partial p}{\partial t} + \beta p \frac{\partial \phi}{\partial t} \tag{3}$$

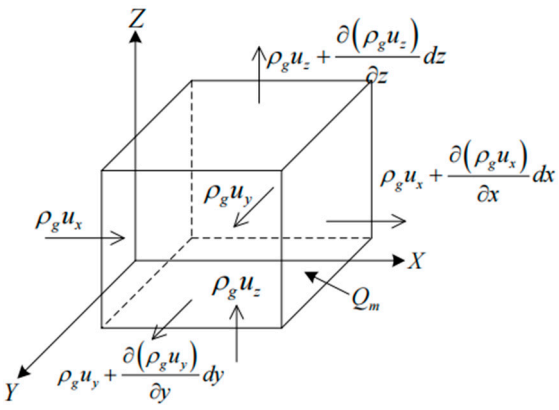


Figure 1. Gas mass conservation in the coal body. Q_m represents the source term, which is taken as 0 in this study; u_x, u_y, u_z represent the seepage velocities in the x, y, and z directions, m/s; $\rho_g u_x$, $\rho_g u_y$, $\rho_g u_z$ represent the seepage fluxes in the x, y, and z directions, in $kg/(m^2 \cdot s)$.

In the equation:

a is the limiting adsorption capacity, m^3/t;

b is the gas adsorption constant, MPa^{-1};
p is the gas pressure, Pa;
ρ_c is the coal body density, kg/m^3;
ρ_0 is the gas density under standard atmospheric pressure, kg/m^3;
c is the correction factor, with a range of 0 to 1;
$\beta = \rho_n / p_n$;
ρ_n is the gas density at standard conditions, kg/m^3;
p_n is the gas pressure under standard conditions, Pa.
The final gas flow model equation is obtained as:

$$\left(\frac{c\rho_c\rho_0 ab}{(1+bp)^2} + \beta\phi\right)\frac{\partial p}{\partial t} + \beta p\frac{\partial \phi}{\partial t} - \nabla\left(\frac{k}{\mu}\beta p\nabla p\right) = 0 \quad (4)$$

In this study, it is assumed that the air present within the coal matrix originates solely from the diffusion of atmospheric air from the mining face and surrounding roadways. The governing equation for airflow is thus derived as follows:

$$\phi\frac{\partial p_1}{\partial t} + p_1\frac{\partial \phi}{\partial t} - \nabla\left(\frac{k}{\mu}\beta p\nabla p\right) = 0 \quad (5)$$

In the equation:
p_1 is the air pressure in the coal body fractures, Pa.

3. Permeability Evolution Simulation of Coal Body Ahead of the Mining Face

3.1. Establishment of the Geometric Model

As the coal body located farther from the mining face experiences minimal mining-induced disturbances, this study focuses on the region extending from 0 to 100 m in front of the mining face. The geometric model adopted in this study is illustrated in Figure 2. The model represents a rectangular domain measuring 100 m in length and 26 m in width, with a coal seam thickness of 6 m. A 5 m wide excavation zone is positioned at the leftmost boundary of the model to simulate mining activity.

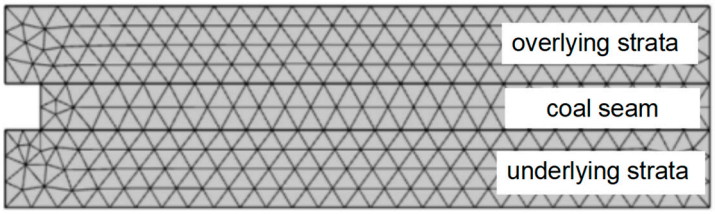


Figure 2. Geometric Model.

3.2. Establishment of the Physical Model

The finite element method is extensively employed to simulate optical, magnetic, and mechanical interactions [30,31]. In this study, COMSOL Multiphysics 6.2 was utilized to simulate the evolution of permeability in the region ahead of the mining face. The simulation incorporated two physics modules—the Solid Mechanics Module and the General Form Partial Differential Equation Module—to capture the coupled interactions among stress, strain, and gas flow within the coal seam. The key simulation parameters for the coal seam are presented in Table 1. The initial gas pressure within the coal seam was set at 1.5 MPa. A uniform load of 5 MPa was applied to the top boundary of the model to simulate the overburden stress, while displacements along the left, right, and bottom boundaries were constrained.

Table 1. Physical Parameters of Coal Seam.

Parameters	Value	Parameters	Value
Apparent density of coal, ρ_c/kg/m^3	1300	Gas density, ρ_0/kg/m^3	0.716
Elastic modulus of coal, E/GPa	2.63	Dynamic viscosity coefficient of gas, u/Pa·s	1.08×10^{-5}
Poisson's ratio of coal, v	0.32	Adsorption constant, a/m^3/t	20
Initial porosity of the coal body, ϕ_0/%	5	Adsorption constant, b/MPa^{-1}	3
Initial permeability of the coal body, k$_0$/m^2	8.61×10^{-16}	Correction coefficient, c	1
Volumetric compressibility coefficient of the coal body, K$_Y$/MPa^{-1}	410		

3.3. Analysis of Simulation Results

Following coal seam excavation, the distribution of vertical stress and corresponding permeability characteristics in the region ahead of the mining face are illustrated in Figure 3. As shown in Figure 3, the vertical stress ahead of the mining face can be categorized into three distinct zones: the pressure-relief zone, the stress concentration zone, and the original stress zone.

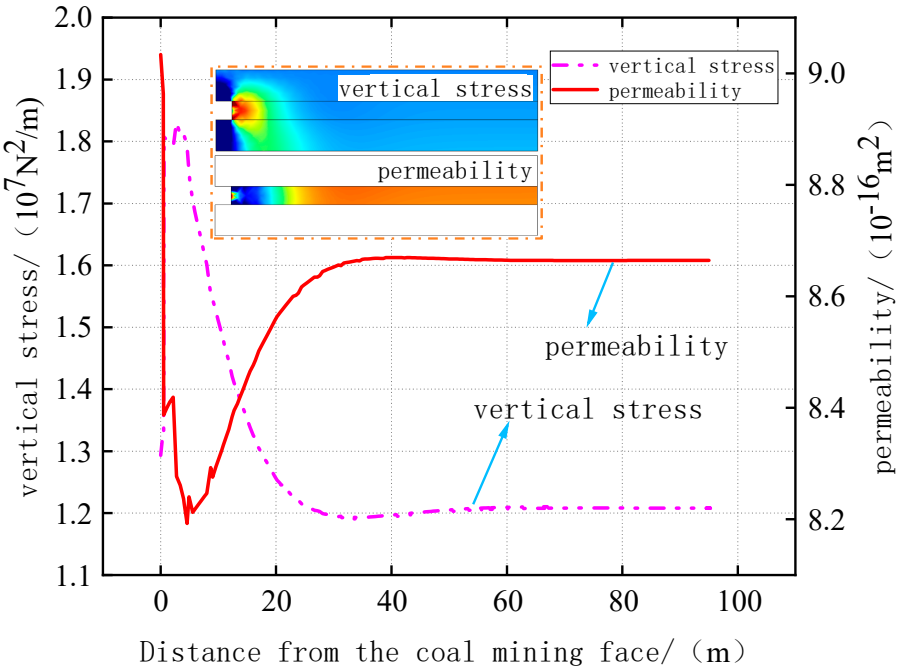


Figure 3. Vertical stress and permeability characteristic curve.

Pressure-relief zone: in this region, the coal seam is initially subjected to high vertical stress, leading to internal compression and fragmentation of the coal matrix. Consequently, vertical stress is alleviated, resulting in increased permeability.

Stress concentration zone: although the vertical stress in this zone remains relatively high, it is insufficient to induce coal failure. The elevated stress compresses fractures within the coal matrix, thereby decreasing permeability. With increasing distance from the mining face, vertical stress gradually diminishes, and permeability correspondingly increases.

Original stress zone: in this region, the vertical stress reflects the in situ stress present prior to mining activities. As the coal matrix remains undisturbed by excavation, its permeability is equivalent to the original in situ value.

4. Study of Gas Drainage Effect Under Different Negative Pressures and Dynamic Negative Pressure Regulation Strategy

To evaluate the influence of varying drainage negative pressures on gas extraction efficiency, three boreholes were strategically positioned within the pressure-relief, stress concentration, and original stress zones ahead of the mining face for simulation analysis. A schematic illustration of the borehole placement is presented in Figure 4.

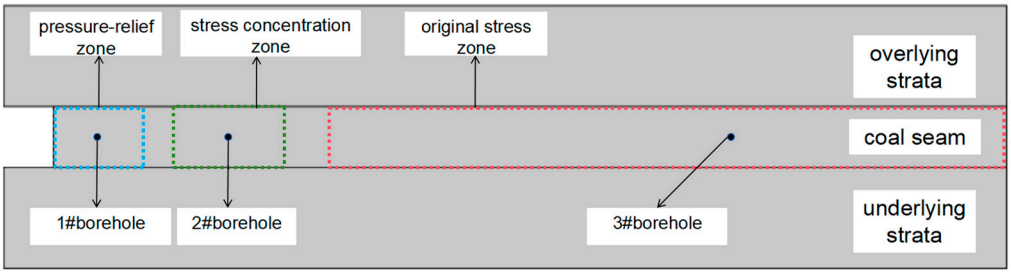


Figure 4. Schematic diagram of gas drainage drilling positions.

4.1. Study on Gas Drainage Effect Under Different Negative Pressures in the Pressure-Relief Zone

The variation trends of the pure gas flow rate and concentration in the borehole located within the pressure-relief zone over the drainage period are illustrated in Figures 5 and 6. As shown in Figure 5, the high permeability of the coal body in the initial phase of gas drainage significantly enhances gas flow. However, as the gas pressure rapidly declines, the pure gas flow rate correspondingly decreases. Higher negative pressure levels accelerate the decline in the pure gas flow rate. Specifically, within the first 0–20 days of drainage, the pure gas flow rate declined by 1.52 m^3/min, 1.59 m^3/min, and 1.88 m^3/min under negative pressures of 13 kPa, 18 kPa, and 25 kPa, respectively. During the mid-to-late stages of drainage, as gas extraction continues to reduce the gas content in the coal matrix, the pure flow rate becomes relatively low. Even with increased negative pressure, the enhancement in the pure gas flow rate remains marginal.

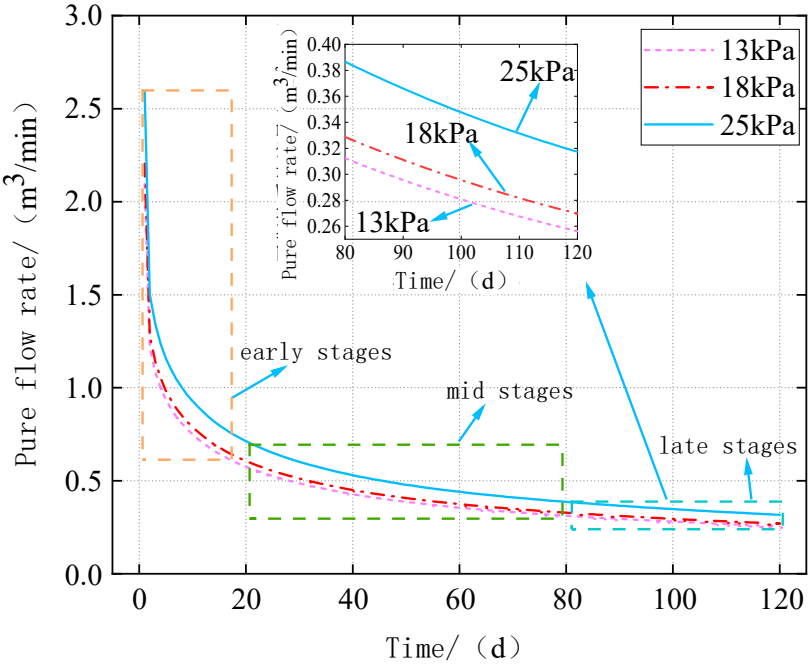


Figure 5. Pure flow rate of gas drainage in the pressure-relief zone.

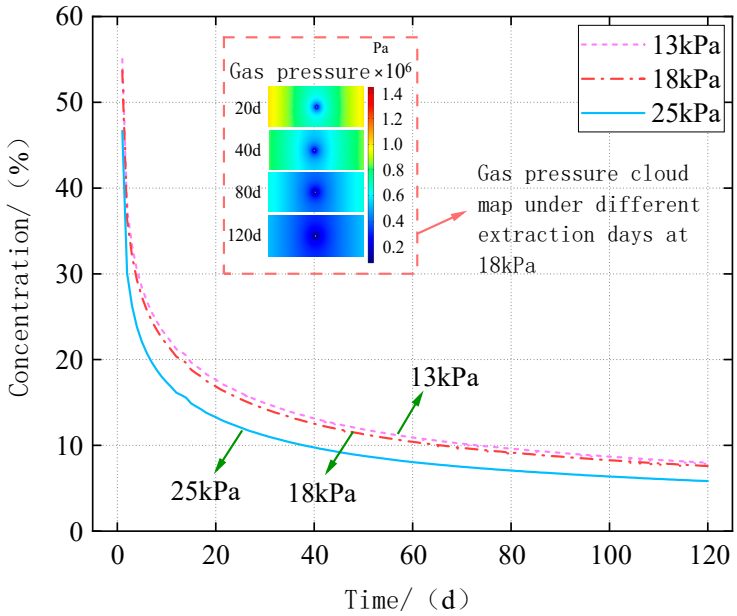


Figure 6. Gas concentration of gas drainage in the pressure-relief zone.

As shown in Figure 6, the high permeability in the pressure-relief zone leads to substantial air leakage from both the mining face and adjacent roadways. The extent of air leakage increases with higher drainage negative pressure. Consequently, during the initial phase of drainage, the gas concentration declines rapidly. In the mid-to-late drainage period, the gas concentration stabilizes at a relatively low level. At 80 days of drainage, gas concentrations under negative pressures of 13 kPa, 18 kPa, and 25 kPa were 9.6%, 9.2%, and 7.1%, respectively.

In the pressure-relief zone, to ensure safe and effective gas extraction, high negative pressure is recommended during the initial drainage phase to reduce the gas content in the coal matrix. As drainage progresses and the pure gas flow rate declines, reducing the negative pressure helps mitigate air leakage and enhance gas concentration. At this stage, gas extraction can be effectively conducted under reduced negative pressure.

4.2. Study on Gas Drainage Effect Under Different Negative Pressures in the Stress Concentration Zone

Figures 7 and 8 illustrate the variations in pure gas drainage flow rate and gas concentration in the borehole located within the stress concentration zone over time.

As shown in Figure 7, during the initial stage of drainage, low permeability causes a slower decline in pure gas flow rate compared to the pressure-relief zone. Under lower negative pressures, the decline in gas pressure is also more gradual. For example, within the first 0–20 days, the pure gas flow rate decreased by 0.35 m^3/min and 0.41 m^3/min under 13 kPa and 18 kPa, respectively. However, under a higher negative pressure of 25 kPa, the increased pressure differential within the coal matrix reduces the dominant role of permeability in governing gas flow. Instead, the pressure gradient between the drainage negative pressure and the gas pressure in coal fractures becomes the primary driver of gas flow. As a result, the gas pressure declines more rapidly under 25 kPa. In the mid-to-late drainage stages, since the gas content in the coal matrix remains higher than in the pressure-relief zone, increasing the negative pressure can moderately enhance the pure gas flow rate.

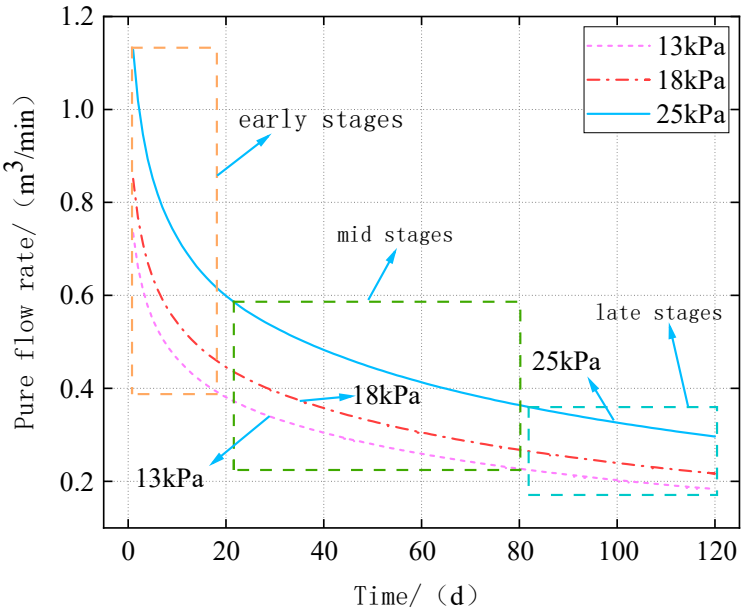


Figure 7. Pure flow rate of gas drainage in stress concentration zone.

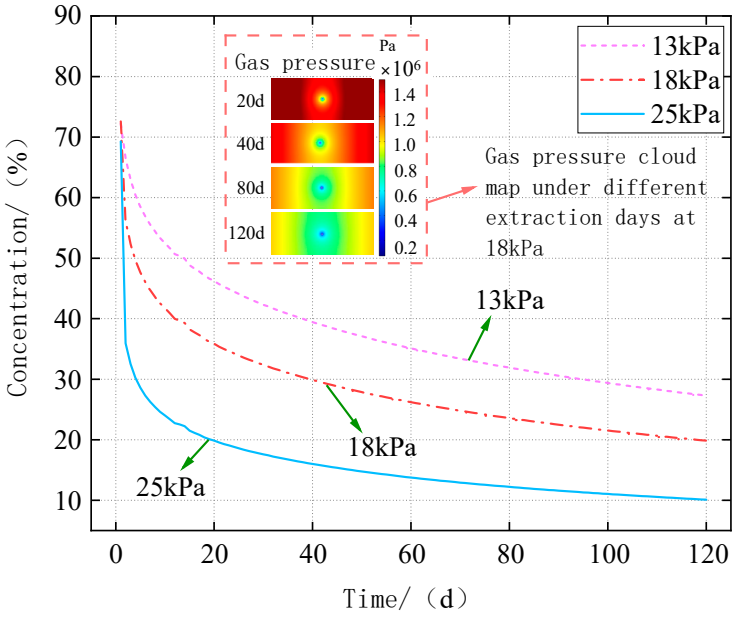


Figure 8. Gas concentration of gas drainage in stress concentration zone.

As shown in Figure 8, due to low permeability and limited air leakage under lower negative pressures, gas concentration decreases more slowly during the early drainage stage than in the pressure-relief zone. Furthermore, in the mid-to-late stages, gas concentration tends to stabilize at relatively higher levels. After 80 days, gas concentrations under 13 kPa and 18 kPa were 31.9% and 37.1%, respectively. However, under 25 kPa, although the pure gas flow rate was higher, the intensified air leakage due to the elevated negative pressure accelerated the decline in gas concentration. Within the first 20 days, the gas concentration dropped by 45.6%, reaching 12.2% by day 80. In the stress concentration zone, high negative pressure should be applied during the initial drainage stage to effectively reduce the gas content in the coal matrix. In the mid-to-late stages, once the gas content falls below the safety threshold and gas concentration declines, reducing the negative pressure can help improve gas concentration levels.

4.3. Study on the Effect of Different Negative Pressures on Gas Drainage in the Original Stress Zone

Figures 9 and 10 illustrate the variation in pure gas drainage flow rate and gas concentration in the borehole within the original stress zone over the drainage period.

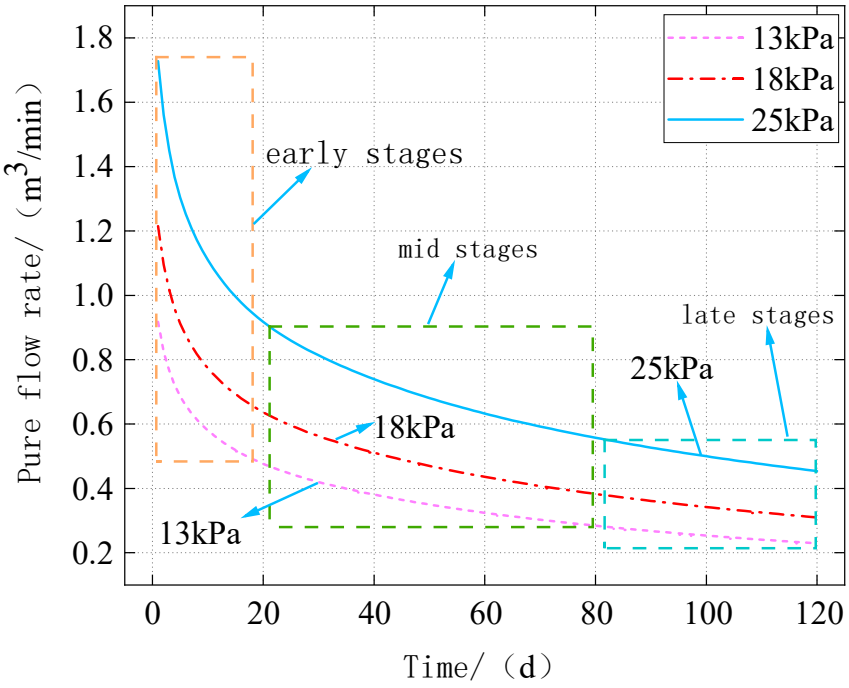


Figure 9. Pure flow rate of gas drainage in the original stress zone.

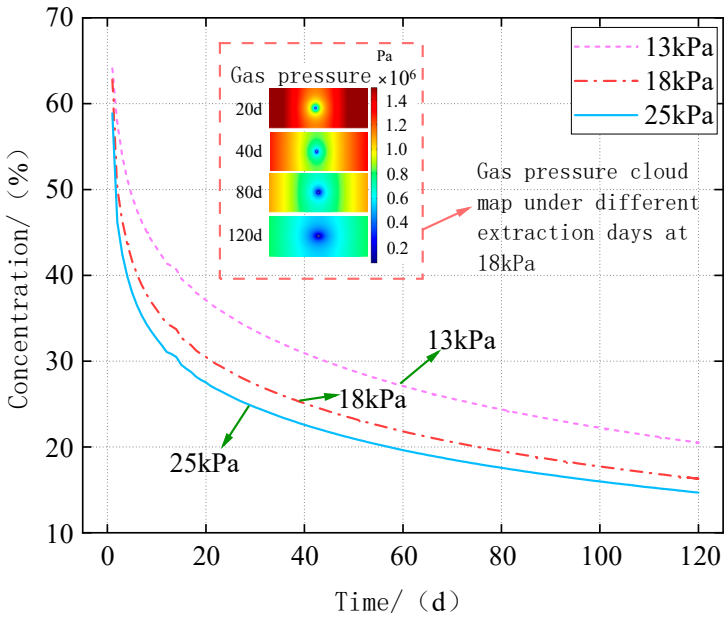


Figure 10. Gas concentration of gas drainage in the original stress zone.

As shown in Figure 9, since the original stress zone remains unaffected by mining disturbances, the permeability of the coal matrix retains its initial state. Gas flow primarily occurs through pre-existing fractures in the coal. Regarding the early stage of drainage, the large pressure differential between the internal gas pressure and the drainage negative pressure causes a rapid decline in gas pressure, leading to a sharp drop in the pure gas flow rate. The higher the applied negative pressure, the faster the decline. For instance,

under negative pressures of 13 kPa, 18 kPa, and 25 kPa, the pure gas flow rates decreased by 0.45 m^3/min, 0.58 m^3/min, and 0.81 m^3/min, respectively, during the first 0–20 days. In the mid-to-late stage of drainage, as the pressure differential gradually decreases, the rate of decline in gas flow slows. However, due to the relatively stable gas content in the coal, the flow rate stabilizes at a relatively high level. Further increasing the negative pressure can enhance gas drainage efficiency during this phase.

According to Figure 10, although the original stress zone is unaffected by mining activity, air leakage from the roadway into the borehole still occurs. In the early stage, with permeability remaining at its initial level, the gas concentration decreases more rapidly than in the stress concentration zone. In the mid-to-late stage, as the gas flow rate decreases and air leakage intensifies, the gas concentration remains at a low level. Lowering the negative pressure reduces air leakage and improves gas concentration. For example, at 80 days of drainage, reducing the negative pressure by 5 kPa and 7 kPa resulted in gas concentration increases of 4.8% and 1.9%, respectively.

In the original stress zone, during the early stage, applying higher negative pressure is effective in reducing gas content in the coal. In the mid stage, moderately lowering the negative pressure helps maintain a higher gas concentration. In the late stage, when both gas pressure and gas content are significantly reduced, minimizing the negative pressure effectively improves gas drainage concentration.

4.4. Research on Intelligent Dynamic Regulation Strategy for Gas Drainage Negative Pressure

Based on the relationship between drainage negative pressure and gas drainage concentration obtained in the preceding analysis, this study proposes an intelligent dynamic control strategy for regulating drainage negative pressure. The Long Short-Term Memory (LSTM) prediction algorithm, a widely used model in big data forecasting, is adopted to predict optimal drainage negative pressure over time. Numerical simulation results, together with field-measured drainage data, are used to construct the training dataset for the LSTM model. After undergoing supervised training, the algorithm is capable of dynamically predicting the optimal negative pressure values to enhance drainage efficiency and gas concentration. On the basis of the prediction outcomes, an intelligent, adaptive regulation framework for drainage negative pressure is established. The complete process of intelligent dynamic control is illustrated in Figure 11.

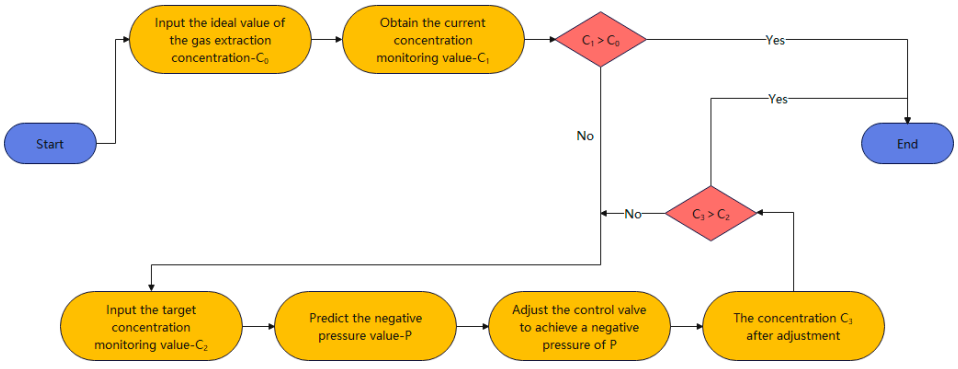


Figure 11. Flow chart of intelligent drainage negative pressure dynamic control.

The intelligent dynamic regulation process for gas drainage negative pressure is outlined as follows:

First, an ideal gas drainage concentration value (C_0) is set as the control target. The actual on-site monitored concentration (C_1) is then collected and compared with C_0. If $C_1 \geq C_0$, no adjustment is required. However, if $C_1 < C_0$, the system enters the concentration regulation mode.

A target concentration value (C_2) is then defined and input into the system. Using the LSTM prediction algorithm, the corresponding optimal drainage negative pressure is forecasted based on the given target concentration.

The system then regulates the drainage valve accordingly, adjusting the negative pressure to the predicted value. After regulation, the new concentration (C_3) is monitored. If $C_3 \geq C_2$, the regulation is considered successful, and the process ends. Otherwise, if $C_3 < C_2$, the regulation is deemed insufficient, and the cycle is repeated until the desired concentration is achieved.

During the drainage process, factors such as mining-induced disturbances and deterioration in borehole sealing may affect gas drainage performance. If multiple regulation attempts fail to meet the target concentration, the system will revise the target value (C_2) and initiate a new adjustment cycle accordingly.

5. Field Application

To validate the accuracy of the above research and assess the applicability of the proposed dynamic regulation strategy for drainage negative pressure, intelligent gas drainage regulation was implemented on-site. Control valves were installed in the pressure-relief zone, stress concentration zone, and original stress zone along the belt roadway of the working face.

A schematic diagram of the valve installation layout is presented in Figure 12, and the actual field installation is shown in Figures 13 and 14.

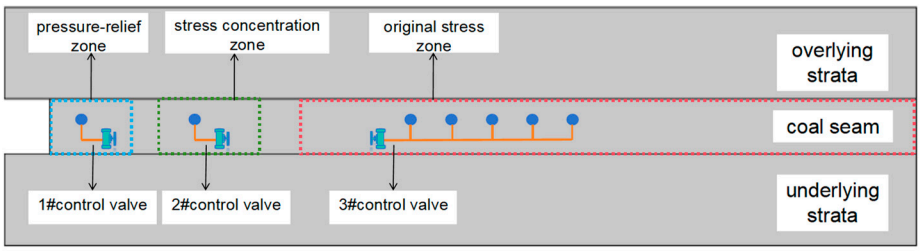


Figure 12. Schematic diagram of valve installation position.

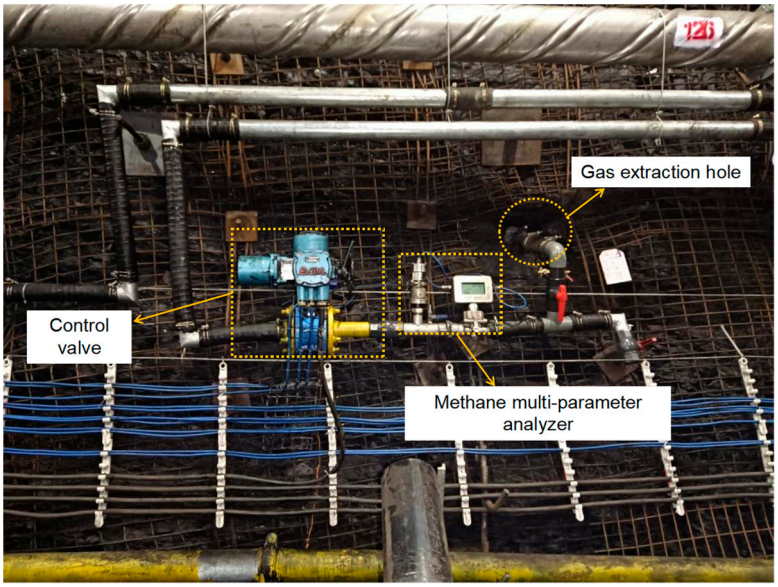


Figure 13. Schematic diagram of single hole installation.

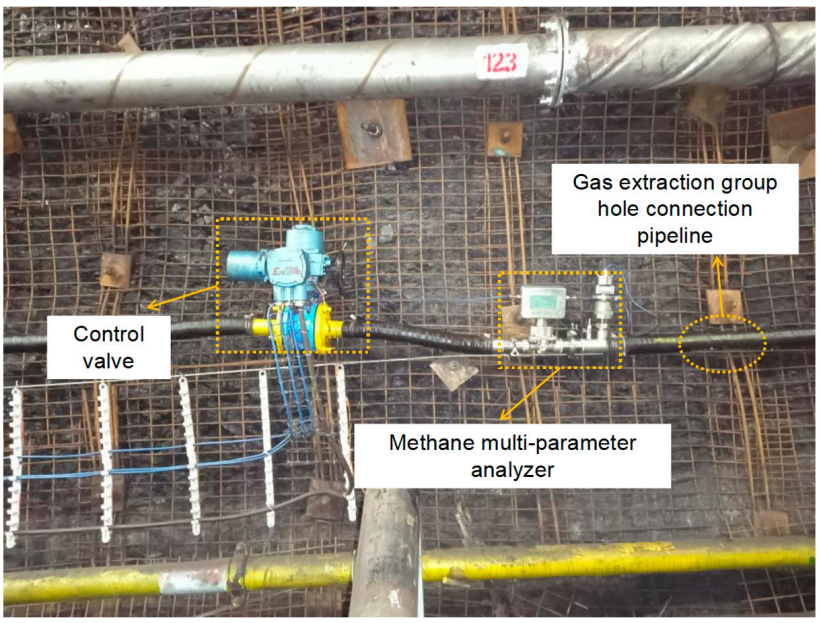


Figure 14. Schematic diagram of parallel holes installation.

Due to the relatively narrow strike widths in the pressure-relief and stress concentration zones, single-hole drainage systems controlled by valves were implemented in these areas. In contrast, the original stress zone, characterized by a wider strike, employed a group-hole drainage approach with valve-based control.

To accurately monitor variations in gas drainage negative pressure and concentration, a methane multi-parameter detector was installed upstream of each valve to measure both parameters in real time. All valves and detectors were integrated with an underground programmable logic controller (PLC) control cabinet. The PLC system transmitted real-time monitoring data to the surface gas drainage monitoring platform, which could also send control commands back to the PLC, thereby enabling remote surface-based regulation of underground valves.

During the trial, gas drainage concentrations were recorded every five days. The target drainage concentration value, C_0, was set at 20%. When measured concentrations fell below this threshold, dynamic regulation of the drainage negative pressure was triggered to restore concentration levels. Regulation was achieved by adjusting the valve opening—reducing the opening effectively lowered the drainage negative pressure.

Gas drainage concentrations were recorded at 5-day intervals throughout the 120-day field trial, with the results presented in Figure 15.

In the stress concentration zone, the gas drainage concentration first fell below the threshold of 20% at day 20. Utilizing the LSTM prediction algorithm to determine the appropriate negative pressure, the valve opening was adjusted to 72%. This adjustment resulted in a wellhead negative pressure of 20.3 kPa and an increase in gas drainage concentration to 32.1%. As drainage progressed, the concentration again dropped below 20% at day 80. A subsequent LSTM-based adjustment reduced the valve opening to 54%, achieving a wellhead negative pressure of 15.6 kPa and raising the concentration to 30.8%.

In the original stress zone, the gas concentration declined below 20% at day 60. Following LSTM prediction, the valve opening was adjusted to 67%, resulting in a concentration increase to 25.3%. At day 80, a further reduction in the valve opening size to 46% improved the concentration to 26.9%.

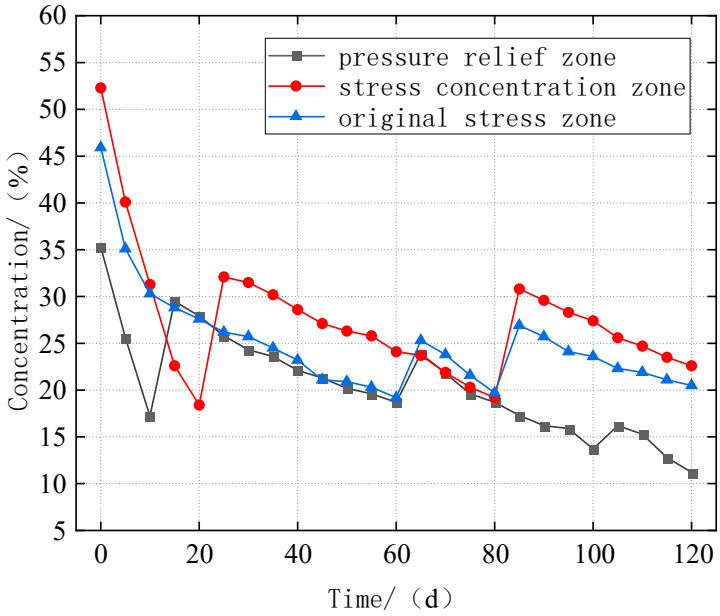


Figure 15. Experimental results.

In the pressure-relief zone, reducing the valve opening in the early stages of drainage significantly enhanced gas concentration. However, in the mid-to-late stages, increased air leakage from the working face and roadway weakened the regulation effect. Although further reductions in valve opening continued to improve gas concentration, the rate of improvement diminished and plateaued at relatively lower levels.

The results of the field trial closely matched the outcomes predicted by numerical simulation. Moreover, the application of LSTM-predicted negative pressure values effectively enhanced gas drainage concentrations. These findings validate the feasibility and practical applicability of the proposed intelligent dynamic regulation strategy for gas drainage negative pressure.

6. Discussion

With the advancement of electronic information and intelligent technologies, numerous traditional manual tasks in coal mining have been effectively automated. In recent years, intelligent mining has experienced rapid development, particularly in areas such as autonomous extraction and disaster prevention and control, where significant breakthroughs have been achieved. Although the adoption of intelligent technologies entails higher initial investments in terms of equipment and infrastructure compared to conventional methods, these technologies substantially enhance both production efficiency and operational safety.

However, as many of these technologies are still in the developmental phase, certain systems remain immature and require further refinement and validation. To accelerate their adoption, two critical aspects must be addressed. First, it is necessary to improve the reliability and robustness of intelligent mining technologies through continuous innovation, thereby expanding their applicability across diverse geological and operational conditions. Second, efforts should be directed toward reducing implementation and maintenance costs, making the technologies more accessible and economically viable for a broader range of mining operations.

By fostering a positive feedback loop between technological advancement and practical application, the coordinated progress of intelligent mining systems and coal mine

production can be effectively promoted, ultimately leading to a safer, more efficient, and sustainable mining industry.

7. Conclusions

(1) Numerical simulation results reveal that permeability and drainage negative pressure are the two primary factors influencing gas flow within the coal seam. When the drainage negative pressure is below a certain threshold, gas flow is predominantly controlled by the permeability of the coal. However, once the negative pressure exceeds this threshold, it becomes the dominant factor governing gas migration.

(2) Based on the quantitative relationship between drainage negative pressure and gas concentration derived from simulation studies, an intelligent dynamic regulation strategy for gas drainage was developed using the LSTM prediction algorithm. This strategy offers a robust theoretical framework for real-time, intelligent adjustment of drainage parameters, enhancing the adaptability and responsiveness of gas control systems in underground coal mines.

(3) Engineering field trials confirmed the feasibility and practicality of the proposed intelligent regulation strategy. The system not only significantly improved gas drainage efficiency but also optimized resource utilization by preventing excessive negative pressure application. These results underscore the potential of intelligent technologies to advance gas drainage practices, thereby supporting the broader development of intelligent mining systems.

Author Contributions: Conceptualization, X.C.; methodology, C.C.; validation, X.C., H.W. and L.X.; formal analysis, C.C.; investigation, X.M.; resources, C.C.; data curation, X.M.; writing—original draft preparation, X.C.; writing—review and editing, H.W.; visualization, C.C.; supervision, L.X.; project administration, X.C.; funding acquisition, X.C. All authors have read and agreed to the published version of the manuscript.

Funding: This research is funded by the National Key Research and Development Program of China, grant number 2023YFF0615404.

Data Availability Statement: The data used to support the findings of this study are available from the corresponding author upon request.

Conflicts of Interest: Authors Xiaoyu Cheng, Cheng Cheng, Lu Xiao and Xingying Ma were employed by the China Coal Energy Research Institute Co., Ltd. Author Hui Wang was employed by the Shaanxi Qinan Coal Mine Safety Evaluation Services Limited. The remaining authors declare that the research was conducted in the absence of any commercial or financial relationships that could be construed as a potential conflict of interest. The China Coal Energy Research Institute Co., Ltd. and Shaanxi Qinan Coal Mine Safety Evaluation Services Limited had no role in the design of the study; in the collection, analyses, or interpretation of data; in the writing of the manuscript, or in the decision to publish the results.

References

1. Fan, C.; Li, S.; Luo, M.; Yang, Z.-H.; Zhang, H.-H.; Wang, S. Deep CBM extraction numerical simulation based on hydraulic-mechanical thermal coupled model. *J. China Coal Soc.* **2016**, *41*, 3076–3085.
2. Zhou, A.; Wang, K.; Wu, Z.; Li, S. Research on airflow catastrophic law induced by gas pressure in min. *J. China Univ. Min. Technol.* **2014**, *43*, 1011–1018.
3. Yao, Y.; Wang, Y.; Wu, Y. Research on measurement of extraction radius based on gas content of coal seam and drilling gas flow. *China Min. Mag.* **2020**, *29*, 116–120+128.
4. El Hachem, K.; Kang, M. Reducing oil and gas well leakage: A review of leakage drivers, methane detection and repair options. *Environ. Res. Infrastruct. Sustain.* **2023**, *3*, 012002. [CrossRef]
5. Uddin, J.; Dubey, R.; Balasubramaniam, V.S.; Kabel, J.; Khare, V.; Salimi, Z.; Sharma, S.; Zhang, D.; Yap, Y.K. Progress in electronic, energy, biomedical and environmental applications of boron nitride and MoS_2 nanostructures. *Micromachines* **2024**, *15*, 349. [CrossRef] [PubMed]

6. Wu, B.; Lei, B.; Hua, M.; Gua, H.; Zhao, Z. Parameters of gas tube extraction technology in the upper corner of working face. *J. Min. Saf. Eng.* **2014**, *31*, 315–321.
7. Zhang, W.; He, Z.; Kong, J.; Zhang, R.; Kang, J. Analysis of influencing factors on gas drainage effect of coal seam boreholes. *China Min. Mag.* **2023**, *32*, 98–102.
8. Liu, X. Numerical simulation and field application of sealing depth of gas extraction borehole in bedding. *China Min. Mag.* **2023**, *32*, 386–390.
9. Li, Q.; Xu, C.; Liu, J.; Fang, J.; Zhang, J.; Liu, F. Key technology and practice of directional drilling for gas drainage in all the mining time and space in underground coal mine. *J. China Coal Soc.* **2022**, *47*, 3108–3116.
10. Wang, L.; Liao, X.; Chu, P.; Zhang, X.; Liu, Q. Study on mechanism of permeability improvement for gas drainage by cross-seam cavitation borehole. *Coal Sci. Technol.* **2021**, *49*, 75–82.
11. Wang, D. Study on dynamic coupling law between drilling extraction radius and pre-pumping period in coal seam. *China Min. Mag.* **2020**, *29*, 144–148.
12. Zhang, H.; Qin, Y.; Su, W. Study on influence mechanism of negative pressure on gas drainage effect. *Saf. Coal Mines* **2019**, *50*, 23–26+31.
13. Lin, H.; Ji, P.; Kong, X.; Li, S.; Dou, G.; Li, K. Precise borehole placement model and engineering practice for pre-draining coal seam gas by drilling along seam. *China Coal Soc.* **2022**, *47*, 1220–1234.
14. Ji, C.; Cui, H. Key technology and practice of gas extraction in steep extra-thick coal seam. *Min. Saf. Environ. Prot.* **2021**, *48*, 99–103.
15. Xu, C.; Wang, J.; Du, C.; Zhou, A.; Wang, K. Simulation of attenuation mechanism of negative pressure along the hole length of long boreholes in gas drainage and its influencing factors. *J. Min. Saf. Eng.* **2021**, *38*, 419–428.
16. Zhang, C.; Gao, X.; Wang, S.; Ren, L. Experimental study and application of the influence of fracture development direction of coal seam on gas extraction effect. *Coal Eng.* **2020**, *52*, 96–100.
17. Lu, W. Research on application and development trend of intelligent technology in mining engineering. *China Min. Mag.* **2024**, *33*, 199–202.
18. He, S.; Wang, N.; Gao, B. Research on intelligent development and application of safety monitoring system based on KJ83X(A). *China Min. Mag.* **2021**, *30*, 149–152.
19. Cheng, Y.; Dong, J.; Li, W.; Chen, M.; Liu, K. Effect of negative pressure on coalbed methane extraction and application in the utilization of methane resource. *J. China Coal Soc.* **2017**, *42*, 1466–1474.
20. Luo, Z.; Zhai, H.; Tong, J. Incorporating multi-features and XGBoost algorithm for gas concentration prediction. *China Min. Mag.* **2024**, *33*, 359–363+370.
21. Wang, Z.; Tian, F.; Zhao, B.; Chen, X.J.; Yu, B.Z. The testing of gas drainage efficiency about feather-veined 1000 m length-drillhole. *J. China Coal Soc.* **2010**, *35*, 76–79.
22. Zhou, F.; Wang, X.; Xia, T. A model of safe drainage of coal seam gas. *J. China Coal Soc.* **2014**, *39*, 1659–1666.
23. Xia, T.; Lu, J.; Li, Z.; Duan, H.; Ren, H.; Zhang, Z.; Zhang, Y. Adaptive control strategy and model of gas-drainage parameters in coal seam. *Sustainability* **2022**, *14*, 9247. [CrossRef]
24. Liu, J.; Liu, Z.; Wei, Y.; Chen, X. Change characteristics of negative drainage pressure along the drill hole: Theoretical analyses and field tests. *ACS Omega* **2022**, *7*, 19948–19956. [CrossRef]
25. Li, C.; Sun, Y.; Wu, S.; Sun, X. Investigation on the gas drainage effectiveness from coal seams by parallel boreholes. *Sustainability* **2023**, *15*, 942. [CrossRef]
26. Zhou, A.; Xu, Z.; Wang, K.; Wang, Y.; An, J.; Shi, Z. Coal mine gas migration model establishment and gas extraction technology field application research. *Fuel* **2023**, *349*, 128650. [CrossRef]
27. Gao, H.; Du, F.; Cheng, X.; Zhang, J.; Zhou, A. Study on the influence mechanism of air leakage on gas extraction effect-a numerical case study of the coal mine site in Anhui. *Processes* **2023**, *11*, 2161. [CrossRef]
28. Zhou, A.; Du, C.; Wang, K.; Fan, X.; Wang, D.; Zhao, W.; Gao, H. Research on intelligent control theory and strategy of gas drainage pipe network based on graph theory. *Fuel* **2024**, *357*, 129867. [CrossRef]
29. Tao, Y.; Xu, J.; Cheng, M.; Li, S.C.; Peng, S.J. Theoretical analysis and experimental study on permeability of gas-bearing coal. *Chin. J. Rock Mech. Eng.* **2009**, *28*, 3363–3370.
30. Amirjani, A.; Abyaneh, P.Z.; Masouleh, P.A.; Sadrnezhaad, S.K. Masouleh finite and boundary element methods for simulating optical properties of plasmonic nanostructures. *Plasmonics* **2022**, *17*, 1095–1106. [CrossRef]
31. Zandi, E.; Alemrajabi, A.A.; Emami, M.D.; Hassanpour, M. Numerical study of gas leakage from a pipeline and its concentration evaluation based on modern and practical leak detection methods. *J. Loss Prev. Process Ind.* **2022**, *80*, 104890. [CrossRef]

Disclaimer/Publisher's Note: The statements, opinions and data contained in all publications are solely those of the individual author(s) and contributor(s) and not of MDPI and/or the editor(s). MDPI and/or the editor(s) disclaim responsibility for any injury to people or property resulting from any ideas, methods, instructions or products referred to in the content.